Dissection of amoeboid movement into two mechanically distinct modes

Kunito Yoshida[1,*] and Thierry Soldati[1,2,‡]

[1]Department of Biological Sciences, Sir Alexander Fleming Building, Imperial College, South Kensington, London, SW7 2AZ, UK
[2]Départment de Biochimie, Faculté des Sciences, Université de Genève, Sciences II, 30 quai Ernest Ansermet, CH-1211-Genève-4, Switzerland
*Present address: School of Biosciences, The University of Birmingham, Edgbaston, Birmingham, B15 2TT, UK
‡Author for correspondence (e-mail: thierry.soldati@biochem.unige.ch)

Accepted 27 June 2006
Journal of Cell Science 119, 3833-3844 Published by The Company of Biologists 2006
doi:10.1242/jcs.03152

Summary

The current dominant model of cell locomotion proposes that actin polymerization pushes against the membrane at the leading edge producing filopodia and lamellipodia that move the cell forward. Despite its success, this model does not fully explain the complex process of amoeboid motility, such as that occurring during embryogenesis and metastasis. Here, we show that *Dictyostelium* cells moving in a physiological milieu continuously produce 'blebs' at their leading edges, and demonstrate that focal blebbing contributes greatly to their locomotion. Blebs are well-characterized spherical hyaline protrusions that occur when a patch of cell membrane detaches from its supporting cortex. Their formation requires the activity of myosin II, and their physiological contribution to cell motility has not been fully appreciated. We find that pseudopodia extension, cell body retraction and overall cell displacement are reduced under conditions that prevent blebbing, including high osmolarity and blebbistatin, and in myosin-II-null cells. We conclude that amoeboid motility comprises two mechanically different processes characterized by the production of two distinct cell-surface protrusions, blebs and filopodia-lamellipodia.

Supplementary material available online at
http://jcs.biologists.org/cgi/content/full/119/18/3833/DC1

Key words: Bleb, Filopodia, Chemotaxis, Osmolarity, Myosin II, Oscillation, *Dictyostelium discoideum*

Introduction

Eukaryotic cells have evolved a wide variety of motility mechanisms, such as the use of ciliae and flagellae, but many, including amoebae and metazoan cells, are able to migrate in three-dimensional substrata by a process known as amoeboid movement (Webb and Horwitz, 2003). This form of motility, common to many adherent cells, results from a combination of myosin contraction at the posterior end and actin polymerization at the anterior end of the cell (Ridley et al., 2003), as well as a cycle of general membrane uptake and localized exocytosis at the advancing anterior membrane (Bretscher, 1996).

Historically, one of the most popular laboratory systems to study cell motility has made use of cultured cells, such as keratocytes, which crawl along a solid two-dimensional substratum. Correlative light and electron microscopy performed sequentially on these moving keratocytes allowed in vivo confirmation of the biochemical mechanisms first dissected in the test tube (Svitkina et al., 1997). These studies culminated in the proposal by Pollard, Borisy and colleagues that, as cells move, a branched network of cortical actin pushes the anterior membrane forward as the actin filaments (F-actin) polymerize at their barbed ends, and that the availability of the free barbed ends limits the polymerization rate – the so-called dendritic nucleation model (reviewed by Pollard and Borisy, 2003). This model appears to explain very well the movement of organelles, bacterial pathogens and artificial particles propelled by actin 'comet tails' in the cytoplasm (Loisel et al., 1999), and it is widely accepted as the major driving force that moves keratocytes, fibroblasts and other cell types (Pollard and Borisy, 2003). Nevertheless, true amoeboid movement is considerably more complex in terms of its morphology and dynamics. For example, simple morphological analysis reveals that the smooth gliding motion of keratocytes (e.g. Anderson et al., 1996) (http://cellix.imolbio.oeaw.ac.at/Videotour/Movies/fig7a.mov) and the step-wise protrusions of crawling embryonic cells (e.g. Dumstrei et al., 2004) (http://www.mtholyoke.edu/courses/rfink/Researchvideopages/rvideo3.htm) must be due to different mechanical processes.

The dendritic nucleation model proposes an important role for actin depolymerization in recycling G-actin for further rounds of polymerization, but it does not predict the apparently inhibitory role of F-actin on cell motility that has been observed in several studies (e.g. Hug et al., 1995; Konzok et al., 1999; Bear et al., 2000; Krause et al., 2002; Strasser et al., 2004; Schirenbeck et al., 2005). Neither does the model predict the existence of two distinct actin networks at the leading edge that have different turnover rates, as was recently demonstrated by fluorescent speckle microscopy of migrating epithelial cells (Ponti et al., 2004) (see also Gupton et al., 2005). Altogether, these studies suggest that profound remodelling of pre-existing cortical actin plays a more prominent role in cell motility than predicted by the dendritic nucleation model.

A situation in which the actin cortex is profoundly remodelled occurs during the well-documented phenomenon of blebbing. Blebs are cell-surface protrusions characterized by

their spherical shape, the lack of visible membrane organelles within them, and their relatively sudden formation, giving the impression that they are local herniations of the plasma membrane (Harris, 1990). Blebs have been observed in many cell types, often associated with unfavourable conditions, such as drug treatment, mutation and apoptosis (Laster and Mackenzie, 1996), but they also accompany physiological processes like mitosis (Laster and Mackenzie, 1996; Boss, 1955; Schroeder, 1978) and development (Trinkaus, 1973). Blebbing cells also migrate: they can move even in the absence of a prominent F-actin layer at the leading edge (Keller and Bebie, 1996; Yoshida and Inouye, 2001), whereas the 'ageing' actin cortex flows towards the centre of the cell and disassembles, as is generally observed during cell locomotion (Yoshida and Inouye, 2001; Grebecki, 1990). The contribution of blebbing to motility deserves further examination.

Bleb formation requires actin and myosin II and it is an active process (Torgerson and McNiven, 1998; Hagmann et al., 1999). Blebbing is thought to occur by expansion of the cytoplasm induced by fluid pressure during a cycle of breakdown and reconstruction of the actin cortex (Harris, 1990; Yoshida and Inouye, 2001; Grebecki, 1990). Myosin II at the posterior end of the cell contracts, increasing the pressure of the cytoplasmic fluid (Mast, 1926; Janson and Taylor, 1993). Blebs form by the action of this pressure on areas of the plasma membrane that have become detached from the cortex by an as yet unknown mechanism (Harris, 1990; Yoshida and Inouye, 2001; Grebecki, 1990; Keller and Eggli, 1998; Keller et al., 2002). Subsequent reconstruction of the actin cortex is thought to stop the advance of the protrusion and/or to stabilize its unsupported membrane (Yoshida and Inouye, 2001; Grebecki, 1990; Keller and Eggli, 1998; Cunningham, 1995; Bereiter-Hahn and Luers, 1998; Keller, 2000; Raucher and Sheetz, 2000).

Much evidence, although not well appreciated, indicates that the hydrostatic pressure of cytoplasmic fluid also plays a role in the motility of various cell types (Keller and Bebie, 1996; Bereiter-Hahn and Luers, 1998; Yanai et al., 1996; Fedier and Keller, 1997; Peckham et al., 2001; Uchida et al., 2003), including the genetically tractable amoeba *Dictyostelium* (Merkel et al., 2000).

In this study, we visualize the dynamics of F-actin in living *Dictyostelium* during both random and chemotactic motion. We demonstrate the involvement of blebbing in amoeboid motility, and we describe the kinetics of two fundamental modes of cell protrusion. We conclude that *Dictyostelium* uses two distinct mechanisms for its motility, a bleb mode and a filopodia-lamellipodia mode. This finding contributes to a more comprehensive and quantitative picture of eukaryotic cell motility and may reconcile former apparent inconsistencies about the role of actin polymerization in this process.

Results

Constitutive blebbing under physiological conditions

In order to monitor actin dynamics at the cell periphery during amoeboid motility, we observed the movement of *Dictyostelium* expressing GFP-ABD (a fusion of green fluorescent protein to the actin-binding domain of ABP120) (Pang et al., 1998). In standard Sörensen buffer (SB) widely used to study amoeba motility, cells that extended pseudopodia (i.e. voluminous protrusions) intermittently formed arc-shaped F-actin structures at their leading edges (Fig. 1A,B are excerpts of the same image sequence, see also supplementary material Movie 1). The protrusions appeared suddenly, emerging within 500 milliseconds with no clear F-actin cortical layer but with a diffuse fluorescence (arrowhead at t=19 seconds in Fig. 1A). This was followed by gradual formation of an F-actin cortical layer under the distended membrane, producing an arc shape (compare t=18.5, 19, and 19.5 seconds in Fig. 1A and arrow in Fig. 1C).

These time-lapse sequences were recorded by epifluorescence and, therefore, the exact shape and location of the pseudopod in three dimensions was determined with a grid confocal microscope (see http://www.thales-optem.com/optigridworks.html). This confirmed constitutive formation of blebs and showed that membrane protrusions usually formed away from the substratum (supplementary material Fig. S1), as had already been shown (Heid et al., 2005). These results explain why bleb formation cannot be visualized using TIRF microscopy (our unpublished results) (Bretschneider et al., 2004).

The arc-shaped structures that we consider as signatures of blebs often appeared between pre-existing or still-growing filopodia (the dense rod-like protrusions containing F-actin) that grow from the pseudopodia (see arrows at t=2 and 3 seconds and arrowheads at 7 seconds in Fig. 1B,C). Under phase-contrast optics, the leading edge of the pseudopodia appears as a hyaline zone devoid of organelles. Multiple, successively formed arcs localized to this hyaline zone and separated it from the cell body, whereas other arcs subdivided the hyaline zone (see t=0 and 1 second in Fig. 1B). Accordingly, staining of a fixed motile cell with Alexa-phalloidin to visualize F-actin illustrated compartmentalization of the pseudopodia (Fig. 2A,B). Kymographs that record the temporal changes in fluorescence intensity along a line scanned repeatedly through the advancing protrusion clearly show the sudden, quantal advances of the leading edge, as well as the gradual appearance of actin arcs. Also, ageing arcs that flowed backwards with respect to the substratum as they disassembled were visualized as nearly horizontal streaks (asterisk at t=5 seconds in Fig. 1C,D). We observed approximately 15 occurrences of the arc-shaped structures during 33 seconds of Movie 1 (0.45 times per second).

We inferred that these membrane protrusions observed in most vigorously moving wild-type cells were blebs because they were hemispherical, appeared suddenly and were initially free of an F-actin cortical layer. To further test this hypothesis, we investigated whether they form in myosin-II-null mutants and in high-osmolarity buffers, in which blebbing is substantially inhibited (Torgerson and McNiven, 1998; Hagmann et al., 1999; Fedier and Keller, 1997; Strohmeier and Bereiter-Hahn, 1987). In myosin-II-null cells (Fig. 1E and supplementary material Movie 2) and in wild-type cells in high-osmolarity buffers (supplemented with more than 100 mM sorbitol, data not shown), the actin staining of the leading edge appeared denser than that in control cells. Numerous filopodia were visible, extending from a flatter protrusion called lamellipodia, but both the arcs and a clearly compartmentalized hyaline zone were lacking from images of both live and fixed cells (Fig. 1E, Fig. 2C,D). We conclude that the membrane protrusions featuring F-actin arcs are indeed blebs.

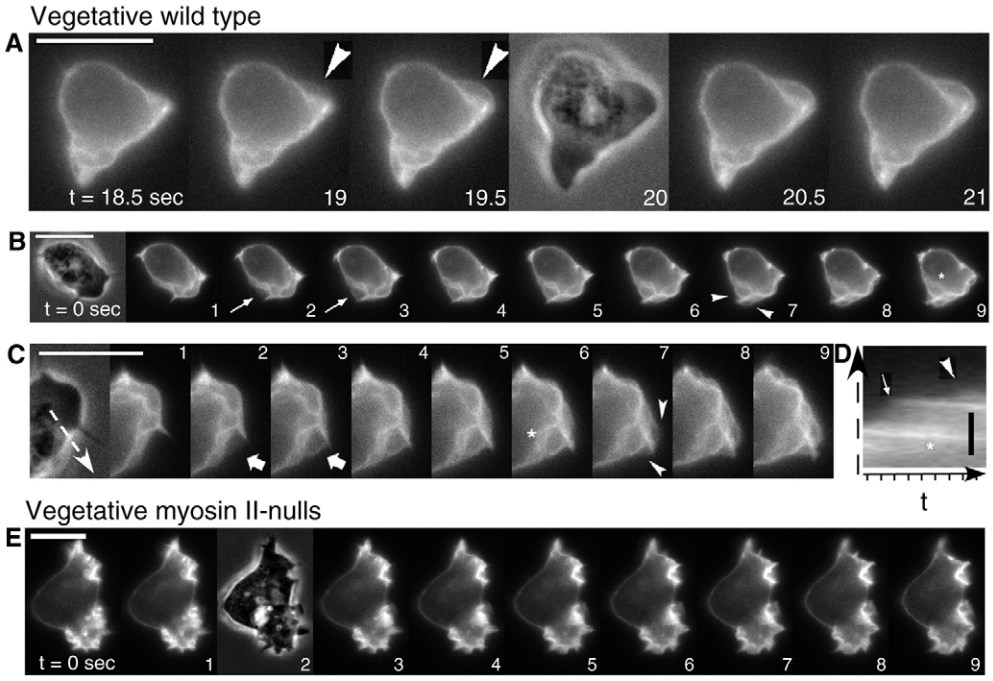

Fig. 1. Microscopy of live vegetative cells expressing GFP-ABD. Fluorescent images of GFP-ABD-expressing, vegetative wild-type (A-D) and myosin-II-null (E) cells in SB were captured sequentially with a CCD camera. (A and B are two excerpts from the same sequence. See supplementary material Movie 1.) Intercalated phase-contrast images are shown at *t*=20 seconds in A, 0 seconds in B, and 2 seconds in E. In A, every frame is shown from left to right. The arrowhead indicates a spherical bleb that formed suddenly; it was initially devoid of F-actin cortex but gradually acquired it. In B, every second frame is shown sequentially from left to right. (C) Higher magnification of the blebbing domain followed in B. The arrow indicates examples of blebs forming beside pre-existing or growing filopodia. The asterisk shows a detached cortical layer moving centripetally. (D) Kymograph obtained by scanning in the direction of the dotted arrow shown in C for the corresponding period. The vertical ticks on the time axis (*t*) are separated by 1 second. The arrow, arrowhead, and asterisk correspond to F-actin layers shown in B and C. (E) Every second frame is shown from left to right. Bars, 10 μm (A-C,E); 3 μm (D).

To finely track pseudopod formation, we observed cells flattened in a silicone oil layer (Fig. 3A) and mapped the time course of membrane velocity (Fig. 3B), F-actin intensity (Fig. 3C), and radial distance (Fig. 3D) at the membrane periphery (see also the combined map Fig. 3E and supplementary material Movie 3). Two major protrusion systems were identified. The first (marked with a red circle in Fig. 3A,D, and shown in higher magnification in supplementary material Fig. S2A) was dominant during the first half of the sequence, with bursts of focal blebs forming repeatedly in the 180° direction (shown as many lateral red streaks in Fig. 3E). Around 60 seconds, the map highlights the emergence of another protrusion in the 270° direction (marked with the green circle in Fig. 3A,D, and magnified in supplementary material Fig. S2B). That protrusion became dominant while the first protrusion system gradually lost blebbing activity and diminished (see Fig. 3A-E). It is remarkable that individual blebs often form in a spatially and temporally correlated sequence: a burst that lasts around one minute. Over the course of many minutes, bursts are primed at random sites of the surface. During bleb formation (arrowheads in Fig. 3B), the F-actin content at the cell boundary (arrowheads in Fig. 3C) was very low, but blebbing was often followed by the emergence of F-actin-rich filopodia growing from a part of the detached cortical actin layer (arrows in Fig. 3A,D and supplementary material Fig. S2B, visible as white streaks in Fig. 3C,D). Overall, approximately 50 unitary blebs were identified as red streaks in Fig. 3E during 135 seconds of the analysis, suggesting an estimated frequency of 0.4 blebs per second in this example. On the other hand, we only found around ten filopodia-like structures during the record period, most of which were persisting over 10-20 seconds.

We also observed similar F-actin arcs in chemotaxing cells at the aggregation stage of development (Fig. 4A,C,E; see supplementary material Movie 4). The blebs formed in a focal manner, in the same general direction as the overall directional movement. A kymograph intersecting the successive blebs can be aligned with a plot of centroid velocity, showing that individual blebs, represented by steps in kymographs, significantly contribute to the peaks in cell movement (Fig. 4C). By contrast, at high osmolarity, the pseudopodia of these developing cells and their actin structures were reminiscent of a neuronal growth cone (Fig. 4B,D,F; see supplementary material Movie 5), with interdigitating lamellipodia and filopodia. In addition, in these samples, we observed that centripetal flow of F-actin layers occurred similarly at both low and high osmolarity, and at intervals of 10-15 seconds (Fig. 4C) and 5 seconds (Fig. 4D), respectively. Notably, in kymographs, the streaks indicating the centripetal flow of detached actin cortices were similarly spaced at intervals of 5 to 10 seconds, irrespective of the conditions (Fig. 1D, Fig. 4C,D), suggesting a common origin.

We conclude that cells have two distinct modes of protrusion, a ‘bleb’ mode that predominates in cells at

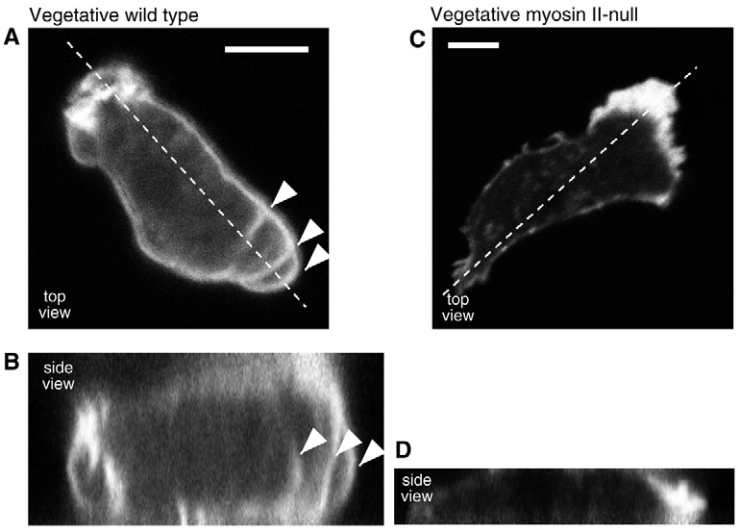

Fig. 2. Visualization of the three-dimensional structure of the actin cortex. Confocal images of fixed wild type (A,B) and myosin-II-null cells (C,D) in SB stained with Alexa Fluor 568-phalloidin to visualize F-actin. (B,D) *Z*-sections along the dotted lines in A and C, respectively. Arrowheads in A and B indicate actin arcs that compartmentalize the protrusion. Bars, 5 μm.

low osmolarity, and a 'filopodia-lamellipodia' mode that predominates in cells at high osmolarity and in myosin-II-null cells, when blebbing is suppressed. In bleb mode, membrane expansion is probably coupled to membrane detachment from the cortex, as was observed in GFP-ABD-expressing cells (Fig. 1A-D, Fig. 3A, Fig. 4A,C,E). The F-actin arcs that form subsequently appear either to stop the further growth of the blebs and/or to stabilize them and build the scaffold for further cell protrusions.

Quantitative analysis of motility in vegetative cells

Our microscopy studies suggested that blebs make a major contribution to cell motility. For example, the bleb indicated by arrowheads in Fig. 1A occupied 3.2 μm^2 (or 5%) of the 63 μm^2 total projected cell area. Blebs usually formed in bursts, adding up to a large protrusive area and thereby determining the direction of cell translocation (see supplementary material Movie 1). To evaluate the contribution of blebbing to physiological cell locomotion, we quantified rates of membrane extension and retraction under conditions that influence blebbing. Accurate 3D microscopy (Heid et al., 2005) is too slow, and sectioning methods such as confocal microscopy, TIRFM and RICM (e.g. Fache et al., 2005) are inappropriate to capture both bleb and lamellipodia-filopodia

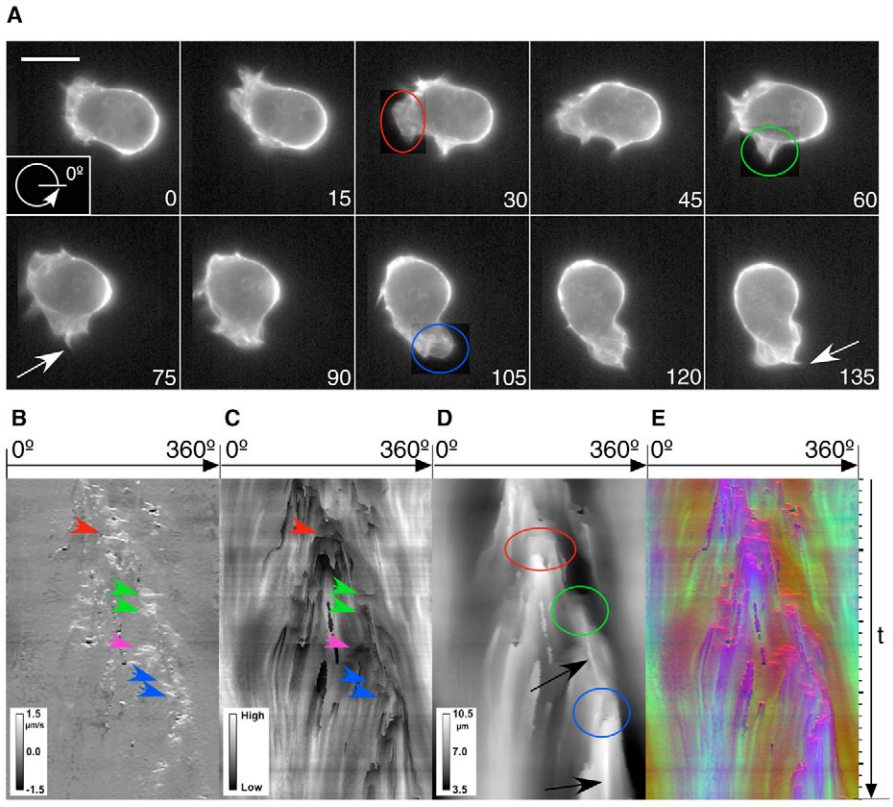

Fig. 3. Spatiotemporal mapping of pseudopod formation. (A) Sequence of fluorescent images of GFP-ABD-expressing, vegetative wild-type cells recorded at intervals of 250 ms and shown every 15 seconds. Bar, 10 μm. (B-E) Cell boundary activity of the cell in A was mapped in polar coordinates (left-right corresponding to 0-360 degrees) along the time axis (from top to bottom over 135 seconds). (B) Membrane velocity, (C) F-actin intensity and (D) radial distance from the centroid. (E) The same images as B-D, coloured in red, green, and blue, respectively were merged. Areas of the protruding sites are shown at higher magnification in supplementary material Fig. S2. To improve appearance of the structures, the original sequence was low-pass filtered at 1 Hz using a windowed-sinc filter (see http://rsb.info.nih.gov/ij/plugins/windowed-sinc-filter.html). Bleb formation was detected as bright areas in B and dark areas in C at the timing of emergence (resulting in red parts in E) as shown with the arrowheads in B, C and supplementary material Fig. S2. The arrows in A indicate persisting filopodia that also appear in D.

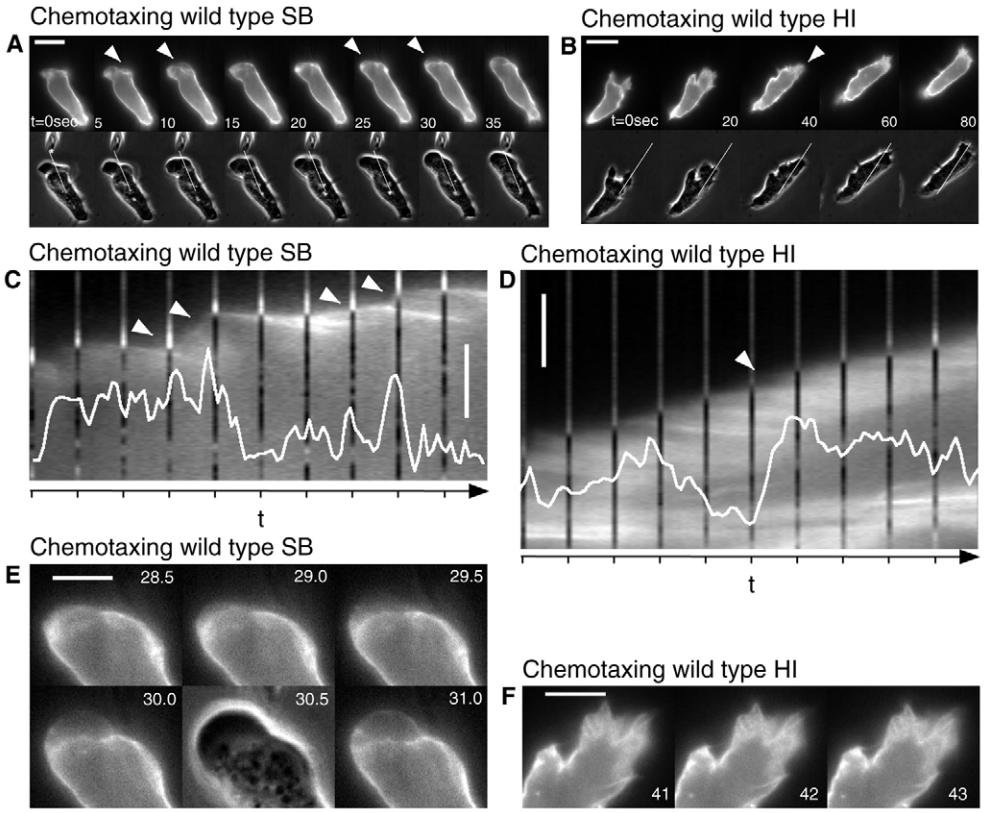

Fig. 4. Microscopy of live chemotaxing cells expressing GFP-ABD. (A-F) Chemotaxing GFP-ABD-expressing cells developed for 8 hours in submerged conditions. (A,B) Fluorescence (top panel) and the corresponding phase-contrast (bottom panel) images at the indicated times. (C,D) Kymographs corresponding to A and B, respectively. Vertical streaks correspond to intercalated phase-contrast images taken every fifth second. The kymographs were aligned and overlaid with plots of the temporal change of centroid velocity calculated from the fluorescent images. Note that the peaks of centroid velocity coincide with bleb formation (arrowheads). A and C were imaged in SB, and B and D in high osmolarity buffer (HI). (C) Spans from –10 to 40 seconds in the sequence shown in A. (D) Spans from 15 to 65 seconds in the sequence shown in B. The arrowheads in A and C indicate a bleb in formation. The arrowheads in B and D indicate a filopodium in formation. (E,F) Higher magnifications of the leading edge of the cells presented in A and B at indicated times. Bars, 10 μm (A,B); 1 μm (C,D); 0.125 μm/second for the centroid velocity plots (C,D); 5 μm in (E,F).

modes. Therefore, we used epifluorescence microscopy of cells expressing cytosolic GFP to obtain a 2D projection image that includes maximal depth information at the necessary time resolution. Image sequences were binarized and the projected cell area gained and lost between successive frames was quantified. Because both motility and blebbing are affected by the osmotic strength of the medium in both *Xenopus* epidermal cells (Strohmeier and Bereiter-Hahn, 1987) and in Walker carcinosarcoma cells (Fedier and Keller, 1997), we examined the impact of osmolarity on membrane extension and retraction rates.

Typical traces of the measured velocities of growth and retraction are shown in Fig. 5. Extension, retraction and movement of the centroid (the calculated centre of mass of the two-dimensional cell projection) showed cyclical acceleration and deceleration, as reported recently by Fache and colleagues (Fache et al., 2005). There were no major differences between wild-type and myosin-II-null cells. The overall kinetic similarity was further confirmed by autocorrelation analysis, which revealed no remarkable difference under the conditions tested (data not shown). However, in wild-type cells in SB, when they form blebs rather than filopodia, it was notable that rapid pulses of extension and retraction frequently coincided (Fig. 5A). This was not observed at high osmolarity or in myosin-II-null cells (Fig. 5B).

This tendency for extension and retraction to coincide in bleb mode conditions was confirmed by cross-correlation analysis. The cross-correlograms have a dull peak at lag 10-20 seconds, suggesting that the gain-of-area has a tendency to precede the loss-of-area by 10-20 seconds, confirming earlier findings of Weber and colleagues (Weber et al., 1995). But exclusively in bleb mode conditions, the cross-correlogram has an extra peak at time lag 0 (sharp red peak at time lag 0, Fig. 5E and magnification in 5F). In filopodia-lamellipodia mode conditions (i.e. at high osmolarity and in absence of myosin II), the cross-correlogram shows no rise at time lag 0 (Fig. 5E,F). This remarkable tendency of simultaneous retraction of the cell body associated with blebbing but not filopodia extension may reflect compensation of cytoplasmic pressure drop upon bleb formation. Histograms of the rates of gain-of-area and loss-of-area were similar (see supplementary material Fig. S3), probably reflecting the overall conservation of cell mass (Dunn and Zicha, 1995).

In wild-type cells, the mean rates of gain-of-area (Fig. 6A) and loss-of-area (Fig. 6B) and the centroid velocities (Fig. 6C) decreased proportionately with the increasing osmolarity of the

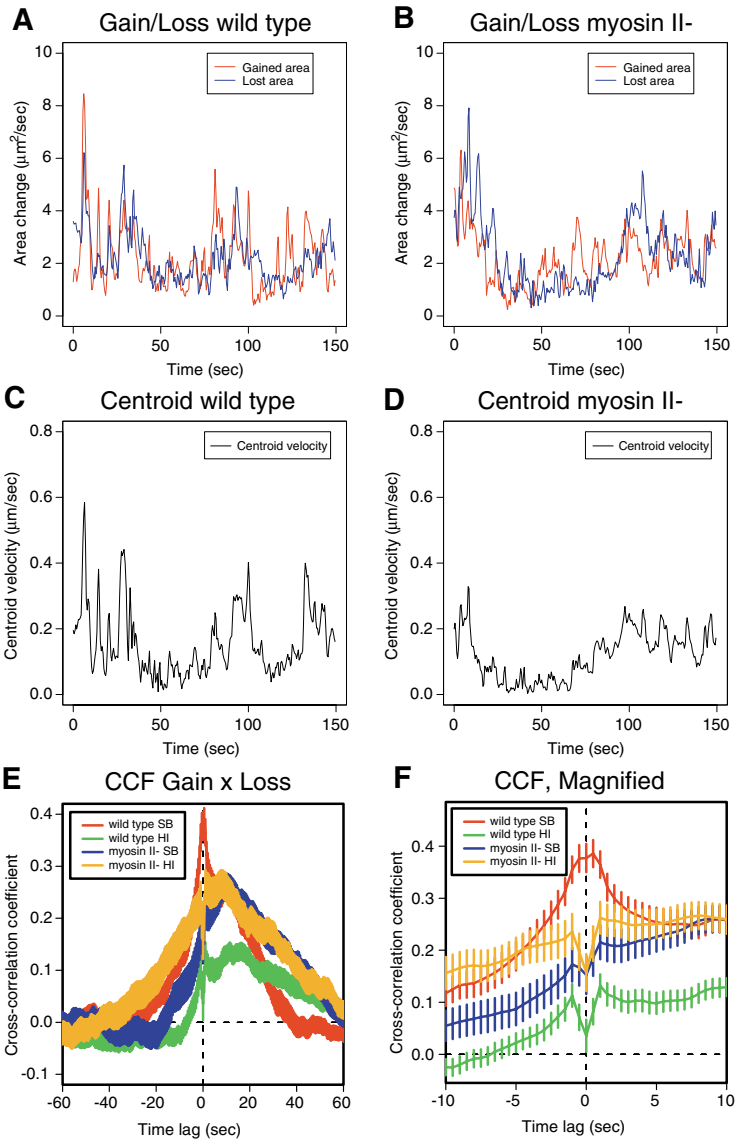

Fig. 5. The oscillatory nature of cell motility. Representative traces of growth rate against time for the cell area gained (red) and lost (blue) (A,B), and the centroid velocity against time (C,D) of vegetative wild-type (A,C) and myosin-II-null (B,D) cells expressing GFP. All cells were imaged in SB. (E) Cross-correlogram between the rates of gain-of-area and loss-of-area are shown for vegetative cells. Cross-correlation (Chatfield, 2003) was calculated with home-developed Perl scripts as the average for each cell population. For a cell sample i, it was defined as:

$$CCF_i(\tau) = \frac{1}{\sigma(G_i)\sigma(L_i)} \cdot \frac{\Sigma_{t=0}^{T_i-\tau}[G(t)-<G>][L(t+\tau)-<L>]}{T_i},$$

where σ (V) indicates the standard deviation of V and T_i is the recording period of the sample i. Area around lag 0 in E is shown at higher magnification in F. Wild-type (WT; red and green) and myosin-II-null (myosin II–; blue and orange) cells in buffer without (SB; red and blue) and with (HI; green and orange) 100 mM sorbitol. The averages of correlation functions from 59 (red), 59 (green), 50 (blue) and 49 (orange) cells are shown. The lines of apparently varying width actually consist of vertical lines representing mean ± s.e.m.

buffer, until they reached half their starting value at 150 mM sorbitol. By contrast, in myosin-II-null cells, all three parameters (Fig. 6A-C) decreased only slightly as the osmolarity increased. Blebbing is observed as a very fast membrane extension (for example, the bleb indicated by arrowheads in Fig. 1A grew at a rate of 6.4 μm^2/second) and such a fast component is missing in the histogram obtained at high osmolarity (see supplementary material Fig. S3), suggesting that reduced occurrence of blebs is the simplest explanation for the suppression of the extension rate by increased osmolarity. Wessels et al. (Wessels et al., 1988) have reported the existence of a fast-moving subpopulation of myosin-II-null cells; therefore we examined various strains of myosin-II-null cells, one of which was as fast as the wild-type strain. We confirmed that the motility of fast myosin-II-null cells was also less influenced by increase of milieu osmolarity (Fig. 6D).

To obtain independent confirmation of the role of myosin II in both bleb formation and motility in wild-type cells, we tested the effects of blebbistatin, an inhibitor of myosin II shown to stop blebbing in human melanoma M2 cells (Straight et al., 2003). Morphological observations performed in SB indicated that blebbing activity was rather promoted in the first 10 minutes of blebbistatin application, but gradually decreased and finally disappeared after 30 minutes, at which time velocity was measured (Fig. 6D). In SB, blebbistatin strongly reduced the velocity of membrane extension of wild-type cells, whereas in myosin-II-null cells it was only slightly decreased (Fig. 6D), suggesting a small non-specific inhibitory effect on myosin-II-null cell motility (Shu et al., 2005). Importantly, blebbistatin abolished the osmolarity sensitivity of wild-type cell motility, confirming the fact that myosin II activity is necessary for blebbing, and hence high-velocity membrane extension.

Dissection of chemotactic motility

In vegetative cells, blebs form in bursts and are restricted to an area of the cell surface for about 1 minute (Fig. 3), resulting in directed locomotion that persists for the same period of time (see supplementary material Fig. S4). At a longer time scale, focal blebbing sites are generated at random, resulting in non-directional overall movement. As already seen in Fig. 4A, blebbing was also observed in chemotaxing cells. But for these

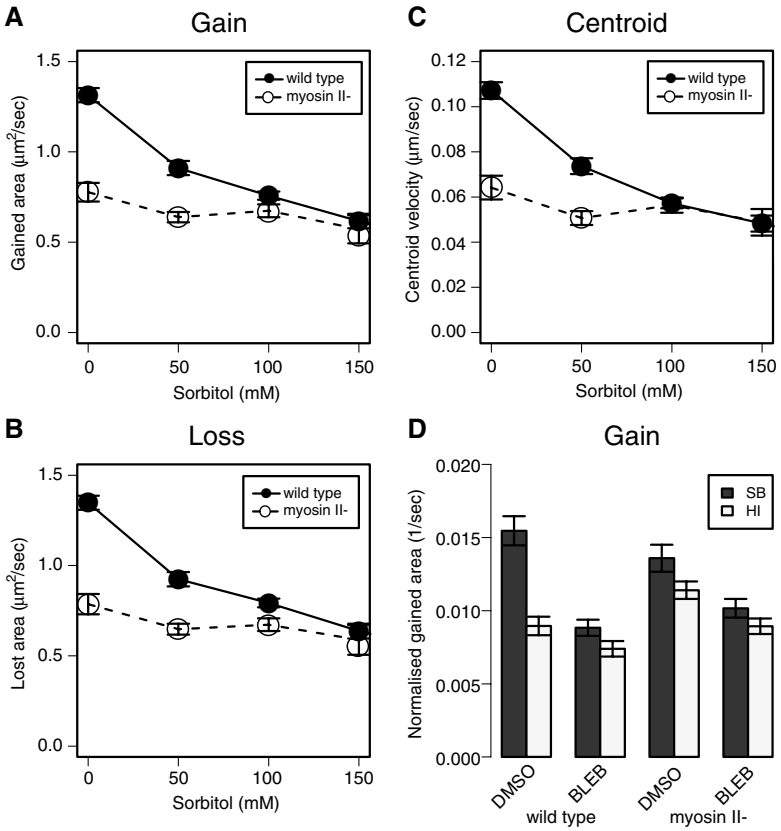

Fig. 6. Effects of buffer osmolarity on velocity of cell movement. The mean values of the rates of gain (A) and loss (B) of cell area, and the centroid velocities (C) are plotted as a function of the sorbitol concentration. Filled symbols, wild type; open symbols, myosin-II-null cells. Data from a slow strain of myosin-II-null cells are shown. Data of various lengths, from 43-149 cells for filled circles and 18-60 for open circles are shown. The error bars indicate the s.e.m. (D) Mean values of the rates of gain-of-area measured in buffers without (SB) or with (HI) 100 mM sorbitol, measured 30-60 minutes after application of 100 μM of blebbistatin (BLEB) or 0.2% DMSO (DMSO). WT and MII- indicate wild type and a fast strain of myosin-II-null cells, respectively. Data were normalized to the mean areas of the corresponding cell and then pooled for statistics (n=22-38 cells).

cells to achieve directed migration, the sites and direction of focal blebbing must be kept under control. Microscopy showed that blebs always formed at the leading edge of chemotaxing cells, i.e. towards the cAMP source (Fig. 4A and supplementary material Movie 4), and therefore their contribution to persistent chemotactic motion was studied further.

In chemotactic wild-type cells, high osmolarity decreased cell speed (Fig. 7E), strongly suggesting that blebbing makes a major contribution to chemotactic motility. Notably, blebbing was also important for aggregation-competent cells randomly moving in the absence of exogenous cAMP gradient, indicating that random and chemotactic movements are powered by identical mechanisms (Fig. 7E). By contrast, the effect of high osmolarity on the chemotactic movement of myosin-II-null cells was small, confirming that the filopodia-lamellipodia mode is the dominant motility mechanism of chemotaxing myosin-II-null cells as was shown for vegetative cells (Fig. 7E).

Analysis of the chemotaxis index (Fig. 7F and its legend) at a short time range (under 80 seconds) showed a clear difference between high and low osmolarity and wild-type and myosin-II-null cells (Fig. 7G). Both wild-type and myosin-II-null cells chemotaxing in high-osmolarity buffer had a tendency to extend more pseudopodia in lateral directions than cells chemotaxing in low-osmolarity buffer; when they began to extend a pseudopodia, the direction of extension deviated from the direction of the cAMP source, and this angle of deviation was larger at high osmolarity, as visualized by representative cell traces (Fig. 7A-D). Observation of GFP-ABD-expressing wild-type cells in high-osmolarity buffer suggested that cells extended filopodia alternately to the left and right of the direction of movement (Fig. 4B and Fig. 7B), as reflected in their low chemotaxis index at a short time range (Fig. 7G). Quantitative analysis indicated that, for wild-type cells, the index values at short time range were 0.75 at low osmolarity and 0.61 at high osmolarity, which correspond to average angle of pseudopodia extension of 41° and 52°, respectively. These indices converged at longer time ranges (over 80 seconds), indicating that contrary to the impact on speed, high osmolarity did not affect the long-range efficiency of wild-type cell chemotaxis. As previously shown (Wessels et al., 1988), chemotaxis of myosin-II-null cells was substantially compromised (Fig. 7C,D,G). At the shortest time range, myosin-II-null cells extended protrusions with an index of 0.57, corresponding to a deviation angle similar to that of wild-type cells at high osmolarity (Fig. 7B). At high osmolarity, chemotaxis of myosin-II-null cells was further impaired, showing more variability in the deviation angles (Fig. 7D,G). At longer time intervals, the indices of myosin-II-null cells increased but never completely converged on those of wild-type cells, reflecting their straying track (Fig. 7C,G).

In conclusion, focal blebbing plays a role in chemotactic movement and, like filopodia extension, is under the control of cAMP signalling.

Discussion

By expressing a fluorescent marker of F-actin and by using high-resolution imaging we have uncovered a role for constitutive plasma membrane blebbing in cell motility, characterized by the appearance of arc-shaped F-actin

structures in the extending pseudopodia. These typical membrane blebs, although already well characterized (Harris, 1990; Yoshida and Inouye, 2001; Grebecki, 1990; Keller and Eggli, 1998), have not previously been widely recognized as playing a role in cell motility. They may have been overlooked for one or more of the following reasons: insufficient temporal or spatial resolution of standard live-imaging systems; inefficiency of conventional fixation techniques in preserving the fragile bleb membrane lacking cytoskeletal support; blebs have been considered to be hallmarks of unhealthy cells (Harris, 1990; Janson and Taylor, 1993; Cunningham, 1995; Mills et al., 1998; Gerisch et al., 1995) and so disregarded; their contribution to motility may have been overshadowed by the success of the dominant model in which actin polymerization directly pushes the leading edge (Condeelis, 1993; Mitchison and Cramer, 1996).

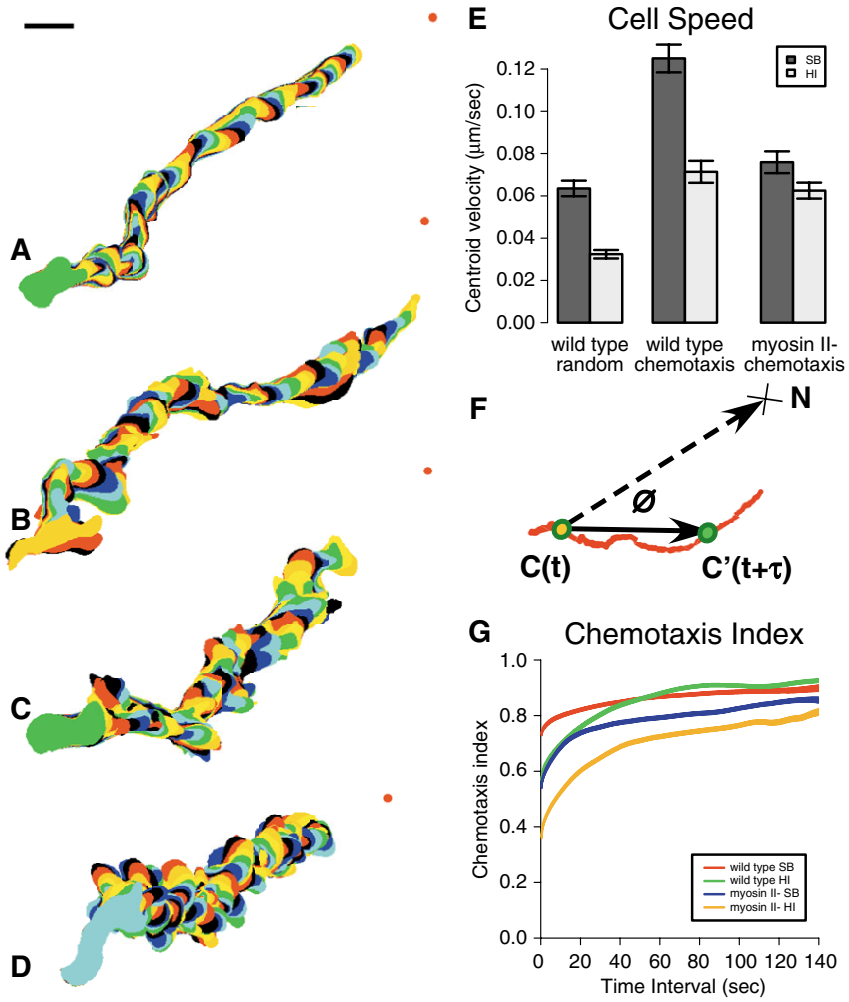

Fig. 7. Effects of osmolarity and myosin II deficiency on directionality of cells during chemotaxis. Representative contour traces of chemotaxing cells at 5-second intervals are shown. (A) AX2 without sorbitol during 535 seconds. Bar, 10 μm. (B) AX2 with 100 mM sorbitol during 525 seconds. (C) A myosin-II-null cell without sorbitol during 465 seconds. (D) A myosin-II-null cell with 100 mM sorbitol during 995 seconds. The red dots at the upper right show the source of the chemoattractant, cAMP. (E) Effects of sorbitol on the velocities of chemotaxing cells. Centroid velocities of cells starved for 8-9 hours were assayed in the absence (random) or presence (chemotaxis) of a capillary filled with 200 μM cAMP. Values are means ± s.e.m. Effects of sorbitol were significant for wild-type cells without or with a cAMP source, but less significant for myosin-II-null cells with a cAMP source. At high osmolarity, the difference between wild-type and myosin-II-null cells in the presence of cAMP was insignificant. (F) For a cell i with the centroid located at a point $C(t)$ at time t moving to a point $C'(t+\tau)$ after time period of τ in the gradient of chemoattractant emitted from the source placed at point N, the chemotaxis index was defined as the mean of $\cos\phi$ weighted by $|\overrightarrow{CC'}|$, with ϕ designating the angle between $\overrightarrow{CC'}$ and $\overrightarrow{CN}$, i.e.

$$CI_i(\tau) = \frac{\Sigma_{t=0}^{T_i-\tau}|\overrightarrow{C(t)C'(t+\tau)}|cos\phi}{\Sigma_{t=0}^{T_i-\tau}|\overrightarrow{C(t)C'(t+\tau)}|}.$$

The average function CI(τ) was calculated with home-developed Perl scripts for a cell population, weighted by the data length T_i–τ. (G) Chemotaxis index shown as a function of time. Wild-type (WT; red and green) and myosin-II-null (MII-; blue and orange) cells in buffer without (SB; red and blue) or with (HI; green and orange) 100 mM sorbitol. The averages of the chemotaxis indices from 56 (red), 42 (green), 44 (blue), and 54 (orange) cells are shown. The line-width represents the means ± s.e.m.

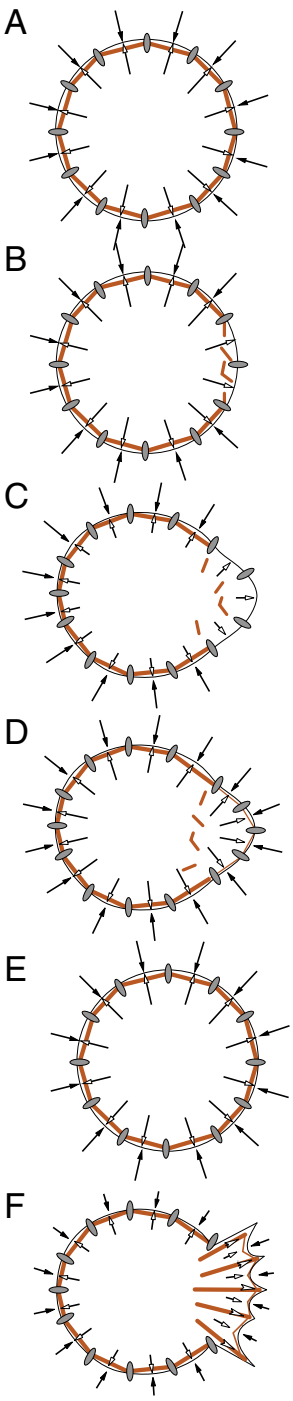

Fig. 8. Model of bleb mode and filopodia-lamellipodia mode motility. (A) At equilibrium, the membrane-cortex system is fully intact and no detachment has occurred. The cytoplasmic pressure is balanced by the pressure resulting from cortical tension. We can write the balance of forces across the cell membrane as:

$$P=2T_c/R\,, \quad (1)$$

$$T_C=T_m+\gamma\,, \quad (2)$$

$$P=\Delta\Pi+P_o\,, \quad (3)$$

where P is the cytoplasmic pressure; T_c, cortical tension, T_m, membrane tension; γ, membrane-cortex adhesion term; and R, radius of the spherical cell. The cytoplasmic pressure consists of two terms, $\Delta\Pi$ the osmotic pressure across the membrane and the remainder P_o a hydrostatic pressure purely due to contraction at $\Delta\Pi$=0. If γ exceeds a threshold value γ_{th}, the membrane will detach from its supporting cortex and a bleb will form (B). This may be achieved either mechanically, through increase of P, or through decrease of γ_{th} due to some biochemical reaction that partially weakens or dissociates the bond. Detachment results in complete dissipation of γ in the corresponding area, which generates a pressure gradient of cytoplasmic fluid across the cell and pushes the detached membrane (C). The initial extension rate would be expected to be proportional to $P–2T_m/R=\Delta\Pi+P_o–2T_m/R$, the differential osmotic pressure, and equal to $2\gamma/R$ the lost adhesion term. In this model, we assume that the cell forms protrusions using energy stored in the equilibrium between inner pressure and cortical tension. Increase of milieu osmolarity would decrease the osmotic gradient, $\Delta\Pi$, and thereby decrease the cortical tension according to equations 1 and 3 above. The decrease in cytoplasmic pressure allows the opposite end of the cell to retract, resulting in net centroid translocation. (D) Finally, a new layer of actin cortex is regenerated and the equilibrium state is restored (E). (F) Myosin-II-null cells move by using a pushing force generated by actin polymerization, without membrane detachment.

Our data show that blebs are intimately associated with the motility of fast-moving amoeboid cells and make a major contribution to the speeds of membrane protrusion and retraction, as well as to the overall centroid velocity. This contribution can be counteracted by increasing the osmolarity of the medium, which slows cell locomotion and inhibits blebbing – an effect that was documented in studies of *Xenopus* epidermal cells (Strohmeier and Bereiter-Hahn, 1987) and Walker carcinosarcoma cells (Fedier and Keller, 1997). It has also been reported that myosin-II-null cells move at less than half the speed of wild-type cells and exhibit a rate of cytoplasmic expansion and contraction roughly half that of wild-type cells (Wessels et al., 1988). Our observations confirm and extend these data, and clearly demonstrate that the motility of myosin-II-null cells is mostly unaffected by the osmolarity of the medium, whereas the velocity of wild-type cells is inversely proportional to the osmolarity. These data suggest that a pressure gradient of cytoplasmic fluid is involved in the motility of wild-type cells but not of myosin-II-null cells.

We conclude that high-speed cell locomotion results from the combination of two basic protrusion modes. In Sörensen buffer of relatively low osmolarity, mainly blebs, but also lamellipodia-filopodia, drive rapid cell extension and determine the direction of cell movement, whereas when myosin II is genetically or pharmacologically inactivated or at high osmolarity, the membrane is probably pushed forward exclusively by actin polymerization. We hypothesize that both blebs and lamellipodia-filopodia can produce a force that displaces the membrane, the dominant mechanism being determined by the balance between internal and external pressures. Consistent with our conclusions, a study of metastasis demonstrated that tumour cells make use of a combination of bleb mode and a mode dictated by actin nucleation followed by polymerization, and implicated the involvement of Rho/ROCK signalling in switching between the two modes (Sahai and Marshall, 2003).

A model for bleb-mode motility

A simple physical model of the forces that power bleb

formation is presented in Fig. 8 and detailed in its legend. We hypothesise that bleb-mode motility is characterized by a rupture of equilibrium (Fig. 8A) generated by focal disruption of the membrane-cortex bond (Fig. 8B) and release of cytoplasmic pressure through a hemispheric distension of the membrane. Since F-actin is not visible in contact with the newly detached membrane, we can suppose that the detached membrane is free from the force generated by actin polymerization (Fig. 8C). The materials necessary for regeneration of the actin cortex are probably initially unavailable in the space between the membrane and the cortex at the time of their dissociation, creating a delay before the regenerated actin cortex can stabilize the membrane (Fig. 8D) and the equilibrium is restored (Fig. 8E). We propose that in the filopodia-lamellipodia mode, no cortical detachment occurs and hence no effective pressure gradient is formed (Fig. 8F). An increase of external osmolarity may result in a decrease of the cytoplasmic pressure under the threshold necessary to rupture the membrane-cortex bond, preventing detachment, and/or slowing down the rate of bleb extension.

The velocity of myosin-II-null cells is not influenced by a range of milieu osmolarity, because no detachment appears to occur, may be partly due to the fact that cortical tension and thus the cytoplasmic pressure of these cells is reduced by half (Pasternak et al., 1989). But this does not fully explain the phenomenon, since a dramatic drop of osmotic pressure could more than compensate for the pressure drop due to myosin II ablation. Previous studies (Shelden and Knecht, 1996) (see also Fig. 2C,E) showed that myosin-II-null cells are much flatter than wild-type cells, suggesting that the apparent elastic modulus of their cortex [or 'poroelastic cytoplasm' (Charras et al., 2005)] is much smaller than in wild-type cells. If it were too extensible, the cortex (or cytoplasm) would easily follow membrane deformation and thus prevent detachment. Accordingly, Laevsky and Knecht showed that cells lacking myosin light chain kinase, in which myosin II has no motor activity but is still capable of actin cross-linking, unlike myosin-II-null cells move normally under restrictive conditions, suggesting that defects in cortical integrity rather than in contraction may be responsible for the motility defects of myosin-II-null cells (Laevsky and Knecht, 2003).

Cross-correlation analysis revealed that, when bleb mode is dominant, the loss-of-area occurred biphasically, one early phase concomitant with the gain-of-area and a late phase lagging 10-20 seconds after protrusion. By contrast, when the filopodia-lamellipodia mode is dominant, the early retraction phase is missing. We suggest that the early retraction phase specifically observed in bleb mode may reflect global mechanical relaxation, compensating the drop of cytoplasmic pressure generated during bleb formation, and may be also relevant to what is referred to as 'circus movement' (Harris, 1990). We also speculate that the commonly observed late retraction phase with a lag of 10-20 seconds occurs as an active process, because a previous study showed that clathrin accumulated in the rear cortex during the corresponding period, probably reflecting a wave of vesicle uptake (Damer and O'Halloran, 2000). The 10- to 20-second-order lags observed in both bleb and filopodia-lamellipodia modes may be explained by the fact that availability of materials such as membrane and adhesion molecules becomes rate limiting.

In conclusion, our observations of randomly moving vegetative cells show that bursts of blebs are primed in random directions. Because the duration of such bursts is about 1 minute, they have a decisive effect on the direction of cell movement. Random orientation of bleb-associated motility is also documented for tumour cells (Sahai and Marshall, 2003). We also observed the formation of blebs in chemotaxing cells but, in this case, the focal bursts appeared to be restricted to the leading edge and contributed to both short- and long-term directionality of movement. Taken together, we conclude that bleb formation is under the control of chemotactic signalling and thus properly orients wild-type cells. Chemotaxis of cells in filopodia-lamellipodia mode was less accurate than bleb mode over a time-scale of less than 1 minute. The protrusions were often produced at an angle to the direction of the cAMP gradient, and the resulting meandering motion was actually exaggerated by increased osmolarity, not only in wild-type cells, but also in myosin-II-null cells. A simple explanation might be that suppression of lateral pseudopod formation is simply related to cortical tension (Heid et al., 2005) irrespective of detachment, and thus does not require myosin II nor does it have a threshold.

Materials and Methods

Cells, vectors and culture conditions

Wild-type cells were from the AX2 strain. We used three strains of myosin II heavy chain null cells, the blasticidin-resistant HS1/AX2 and HS1/Orf1 strains and G418-resistant myosin-II-null cells (gifts from D. Manstein, Hanover University, Germany). The pDXA-GFP-ABD (a gift from D. Knecht, University of Connecticut, Storrs, CT) (Pang et al., 1998) was stably integrated in HS1/AX2 cells, or maintained extrachromosomally in AX2 cells by co-transfection with the pREP vector. Selection was performed in HL5c medium (Sussman, 1987) containing 10 μg/ml G418. For motility analysis, pTX-GFP (a gift of T. Egelhoff, Case School of Medicine, Cleveland, OH) (Levi et al., 2000) was maintained extra chromosomally by selection with 30 or 40 μg/ml G418 for AX2 cells and G418-resistant myosin-II-null cells, respectively. Alternatively, pDXA-GFP was stably integrated in AX2 or HS1/AX2 cells, and selected with 30 μg/ml G418. For chemotaxis assays, the pDXA-GFP was maintained in HS1/Orf1 myosin-II-null cells by selection with 10 μg/ml G418.

Phalloidin staining

Cells incubated in standard buffer (Sörensen buffer or SB: 14.7 mM KH_2PO_4, 2.5 mM Na_2HPO_4, pH 6.2) for 10 minutes were fixed in 1% glutaraldehyde in the same buffer and stained with Alexa Fluor 568-phalloidin as already described (Yoshida and Inouye, 2001). After mounting in ProLong antifade (Molecular Probes, Invitrogen, Paisley, UK) slides were observed with a Leica SP2 confocal microscope using a Plan-Apochromat 63× 1.32 NA oil-immersion Ph3 objective (Zeiss).

Live cell microscopy

Cells were plated on coverslips submerged in HL5c without G418 and incubated overnight. Then, the coverslip was soaked with 17 mM Na/K phosphate buffer pH 6.2 supplemented with the indicated concentrations of sorbitol, and sealed upside-down on a chamber formed by a trough cut into a 1 mm-thick sheet of silicone rubber (a gift from K. Inouye, Kyoto University, Japan) on a glass slide, or alternatively, on a drop of silicone oil (KF-96A, a kind gift of Shin-Etsu Silicones) (Yoshida and Inouye, 2001). To image blebs, AX2 or myosin-II-null cells expressing GFP-ABD were observed by phase-contrast or fluorescence microscopy using a Plan-Apochromat 63× 1.40 NA Ph3 oil-immersion objective (Zeiss, Jena, Germany), and recorded with a CCD camera (Sensicam, PCO AG, Kelheim, Germany) through a 1.25× relay lens using ImageJ Software (NIH; http://rsb.info.nih.gov/ij/) with self-developed plug-in at the specified frame rates (500 or 250 milliseconds). Phase-contrast images were intercalated every 20 frames using shutters (SC-2 Applied Scientific Instrumentation, Eugene, OR) controlled through the capturing plug-in of ImageJ.

2D mapping of membrane activity of a GFP-ABD cell

We expressed the cell edge points in polar coordinates (r, ϕ), with the centroid C as the origin, r the radial distance, and ϕ the polar angle. Thus the radial distance was defined as a function of the origin C, time t, and angle ϕ, i.e. $r(C, t, \phi)$. To calculate the membrane velocity, we first measured the radial distance r in every pair of successive images at t–1 and t+1, with the same centroid at time t–1, i.e.,

C_{t-1}, as the origin. Then the membrane velocity at time t and angle ϕ was calculated as:

$$u(t,\phi) = \frac{r(C_{t-1},t+1,\phi) - r(C_{t-1},t-1,\phi)}{2\Delta t},$$

for 360°. Δt is the time frame (250 milliseconds in this case).

To measure the actual radial distance in GFP-ABD expressing cells, the radial line was scanned outwards to identify the point where the gradient of the square root of the intensity was maximal. (In fact the gradient was calculated for 5×5 pixels surrounding the scanning point.) Then the pixel second next inward to the detected maximum was assigned as the cell edge point, and its intensity was mapped onto the angle-time 2d plane. After obtaining the edge points in every direction, these points were smoothed with a five-sample moving average filter of $r'(\phi_j)=\{r(\phi_{j-2})+r(\phi_{j-1})+...+r(\phi_{j+2})\}/5$. In addition, these five points were fitted by the least square method to obtain the tangential line to the cell contour and thereby its tilt angle to the radial line, and the membrane velocity was corrected to the component normal to the membrane.

Chemotaxis assays

Cells were submerged in 500 μl of 17 mM Na/K phosphate buffer pH 6.2 supplemented with 25 mM KCl, 2.5 mM $MgSO_4$ and 1 mM $CaCl_2$ at a density of 10^7 cells/ml in a 3.5 cm diameter dish. After 8 hours of starvation, the cells were placed on a coverslip at a density of $5\times10^5/28.5$ cm^2. After 20 minutes to allow cell attachment, the coverslip was transferred into a plastic dish containing test buffer, i.e. 17 mM Na/K phosphate pH 6.2 with or without sorbitol. A glass capillary filled with 170 mM Na/K phosphate buffer pH 6.2 containing 200 μM cAMP and 2 mM Fluorescein was placed in the centre of the imaging field. After 5 minutes to allow gradient formation, cells were imaged with an AchroPlan 40× 0.75 NA Ph2 water-immersion objective (Zeiss) at intervals of 1 second for 500 or 1000 frames. To visualize chemotaxis of GFP-ABD-expressing cells, starved cells were transferred into a glass-bottomed plastic culture dish (MatTek, Ashland, MA) containing test buffer, and observed with an inverted total internal reflection fluorescence (TIRF) microscope (Till Photonics, Gräfelfing, Germany) illuminated by a 488 nm laser, using a 100× 1.4 NA Ph3 oil-immersion objective. Contours and centroids of chemotaxing cells were determined by running the 'Analyze Particle' function of ImageJ against the contrast-enhanced stacked images in which areas of interest had been cropped. The centroid velocity was determined from the distance between the centroid positions in the successive frames.

Quantitative analysis of cell motility

GFP-expressing cells were prepared for observation as described above. Ten minutes after sample preparation, cells showed indistinguishable random movements for 1 hour. Images were captured at 500 millisecond intervals for 250 seconds with a 40× 1.30NA Plan-Neofluar Ph3 oil-immersion objective in combination with 2.5× relay lens. Sequential images were processed in the following order using home-made ImageJ plug-ins. (1) The intensity was digitally enhanced to saturate more than 90% of the pixels in the cell area. (2) The image was blurred with Gaussian filter of 5-pixel radius. (3) The threshold was set to 128 and the 'Analyze Particle' function was run to determine the cell centroid and generate a binary image used to guide the calculation of cell boundary. For every i ($1<i<N$) frame, gained and lost areas of cell body projections were determined from the difference of binary images between the frame i+1 and i–1 (Weber et al., 1995; Dunn et al., 1997). The centroid velocity was determined from the distance between the centroid position at i+1 and i–1.

Statistical analyses

The average velocities (the rates of gain-of-area and loss-of-area, and the centroid velocity) were calculated for every cell and analyzed statistically to estimate the means and s.e.m. irrespective of the record length. The calculation was performed by GNU R software.

We thank D. Knecht and T. Egelhoff for plasmids and D. Manstein for kind gifts of plasmids and myosin-II-null strains. We are grateful to M. Peckham, G. Dunn, K. Weijer, B. Fourcade, F. Bruckert, R. Insall and K. Inouye for their helpful discussions, C. Featherstone for critical reading and editing. We thank L. Armstrong and others at Improvision for generous help with grid confocal microscopy, and S. Fraser, D. Ushakov and M. Ferenczi for help with the experimental setups for chemotaxis. The work was supported by grants from the UK Biotechnology and Biological Sciences Research Council, The Wellcome Trust and the Swiss National Science Foundation.

References

Anderson, K. I., Wang, Y. L. and Small, J. V. (1996). Coordination of protrusion and translocation of the keratocyte involves rolling of the cell body. *J. Cell Biol.* **134**, 1209-1218.

Bear, J. E., Loureiro, J. J., Libova, I., Fassler, R., Wehland, J. and Gertler, F. B. (2000). Negative regulation of fibroblast motility by Ena/VASP proteins. *Cell* **101**, 717-728.

Bereiter-Hahn, J. and Luers, H. (1998). Subcellular tension fields and mechanical resistance of the lamella front related to the direction of locomotion. *Cell Biochem. Biophys.* **29**, 243-262.

Boss, J. (1955). Mitosis in cultures of newt tissues. IV. The cell surface in late anaphase and the movements of ribonucleoprotein. *Exp. Cell Res.* **8**, 181-187.

Bretscher, M. S. (1996). Getting membrane flow and the cytoskeleton to cooperate in moving cells. *Cell* **87**, 601-606.

Bretschneider, T., Diez, S., Anderson, K., Heuser, J., Clarke, M., Muller-Taubenberger, A., Kohler, J. and Gerisch, G. (2004). Dynamic actin patterns and Arp2/3 assembly at the substrate-attached surface of motile cells. *Curr. Biol.* **14**, 1-10.

Charras, G. T., Yarrow, J. C., Horton, M. A., Mahadevan, L. and Mitchison, T. J. (2005). Non-equilibration of hydrostatic pressure in blebbing cells. *Nature* **435**, 365-369.

Chatfield, C. (2003). *The Analysis of Time Series: An Introduction*. Florida: CRC Press.

Condeelis, J. (1993). Life at the leading edge: the formation of cell protrusions. *Annu. Rev. Cell Biol.* **9**, 411-444.

Cunningham, C. C. (1995). Actin polymerization and intracellular solvent flow in cell surface blebbing. *J. Cell Biol.* **129**, 1589-1599.

Damer, C. K. and O'Halloran, T. J. (2000). Spatially regulated recruitment of clathrin to the plasma membrane during capping and cell translocation. *Mol. Biol. Cell* **11**, 2151-2159.

Dumstrei, K., Mennecke, R. and Raz, E. (2004). Signaling pathways controlling primordial germ cell migration in zebrafish. *J. Cell Sci.* **117**, 4787-4795.

Dunn, G. A. and Zicha, D. (1995). Dynamics of fibroblast spreading. *J. Cell Sci.* **108**, 1239-1249.

Dunn, G. A., Weber, I. and Zicha, D. (1997). Protrusion, retraction and the efficiency of cell locomotion. In *Dynamics of Cell and Tissue Motion* (ed. W. Alt, A. Deutsch and G. A. Dunn), pp. 33-46. Basel: Birkhauser.

Fache, S., Dalous, J., Engelund, M., Hansen, C., Chamaraux, F., Fourcade, B., Satre, M., Devreotes, P. and Bruckert, F. (2005). Calcium mobilization stimulates Dictyostelium discoideum shear-flow-induced cell motility. *J. Cell Sci.* **118**, 3445-3457.

Fedier, A. and Keller, H. U. (1997). Suppression of bleb formation, locomotion, and polarity of Walker carcinosarcoma cells by hypertonic media correlates with cell volume reduction but not with changes in the F-actin content. *Cell Motil. Cytoskeleton* **37**, 326-337.

Gerisch, G., Albrecht, R., Heizer, C., Hodgkinson, S. and Maniak, M. (1995). Chemoattractant-controlled accumulation of coronin at the leading edge of Dictyostelium cells monitored using a green fluorescent protein-coronin fusion protein. *Curr. Biol.* **5**, 1280-1285.

Grebecki, A. (1990). Dynamics of the contractile system in the pseudopodial tips of normally locomoting amoebae, demonstrated in vivo by video-enhancement. *Protoplasma* **154**, 98-111.

Gupton, S. L., Anderson, K. L., Kole, T. P., Fischer, R. S., Ponti, A., Hitchcock-DeGregori, S. E., Danuser, G., Fowler, V. M., Wirtz, D., Hanein, D. et al. (2005). Cell migration without a lamellipodium: translation of actin dynamics into cell movement mediated by tropomyosin. *J. Cell Biol.* **168**, 619-631.

Hagmann, J., Burger, M. M. and Dagan, D. (1999). Regulation of plasma membrane blebbing by the cytoskeleton. *J. Cell Biochem.* **73**, 488-499.

Harris, A. K. (1990). Protrusive activity of the cell surface and the movements of tissue cells. In *Biomechanics of Active Movement and Deformation of Cells (NATO ASI Series H)*. Vol. 42 (ed. N. Akkas), pp. 249-294. Berlin, New York: Springer-Verlag.

Heid, P. J., Geiger, J., Wessels, D., Voss, E. and Soll, D. R. (2005). Computer-assisted analysis of filopod formation and the role of myosin II heavy chain phosphorylation in Dictyostelium. *J. Cell Sci.* **118**, 2225-2237.

Hug, C., Jay, P. Y., Reddy, I., McNally, J. G., Bridgman, P. C., Elson, E. L. and Cooper, J. A. (1995). Capping protein levels influence actin assembly and cell motility in dictyostelium. *Cell* **81**, 591-600.

Janson, L. W. and Taylor, D. L. (1993). In vitro models of tail contraction and cytoplasmic streaming in amoeboid cells. *J. Cell Biol.* **123**, 345-356.

Keller, H. and Eggli, P. (1998). Protrusive activity, cytoplasmic compartmentalization, and restriction rings in locomoting blebbing Walker carcinosarcoma cells are related to detachment of cortical actin from the plasma membrane. *Cell Motil. Cytoskeleton* **41**, 181-193.

Keller, H., Rentsch, P. and Hagmann, J. (2002). Differences in cortical actin structure and dynamics document that different types of blebs are formed by distinct mechanisms. *Exp. Cell Res.* **277**, 161-172.

Keller, H. U. (2000). Redundancy of lamellipodia in locomoting Walker carcinosarcoma cells. *Cell Motil. Cytoskeleton* **46**, 247-256.

Keller, H. U. and Bebie, H. (1996). Protrusive activity quantitatively determines the rate and direction of cell locomotion. *Cell Motil. Cytoskeleton* **33**, 241-251.

Konzok, A., Weber, I., Simmeth, E., Hacker, U., Maniak, M. and Muller-Taubenberger, A. (1999). DAip1, a Dictyostelium homologue of the yeast actin-interacting protein **1**, is involved in endocytosis, cytokinesis, and motility. *J. Cell Biol.* **146**, 453-464.

Krause, M., Bear, J. E., Loureiro, J. J. and Gertler, F. B. (2002). The Ena/VASP enigma. *J. Cell Sci.* **115**, 4721-4726.

Laevsky, G. and Knecht, D. A. (2003). Cross-linking of actin filaments by myosin II is

a major contributor to cortical integrity and cell motility in restrictive environments. *J. Cell Sci.* **116**, 3761-3770.

Laster, S. M. and Mackenzie, J. M., Jr (1996). Bleb formation and F-actin distribution during mitosis and tumor necrosis factor-induced apoptosis. *Microsc. Res. Tech.* **34**, 272-280.

Levi, S., Polyakov, M. and Egelhoff, T. T. (2000). Green fluorescent protein and epitope tag fusion vectors for Dictyostelium discoideum. *Plasmid* **44**, 231-238.

Loisel, T. P., Boujemaa, R., Pantaloni, D. and Carlier, M. F. (1999). Reconstitution of actin-based motility of Listeria and Shigella using pure proteins. *Nature* **401**, 613-616.

Mast, S. (1926). Structure, movement, locomotion and stimulation in amoebae. *J. Morphol. Physiol.* **41**, 347-425.

Merkel, R., Simson, R., Simson, D. A., Hohenadl, M., Boulbitch, A., Wallraff, E. and Sackmann, E. (2000). A micromechanic study of cell polarity and plasma membrane cell body coupling in Dictyostelium. *Biophys. J.* **79**, 707-719.

Mills, J. C., Stone, N. L., Erhardt, J. and Pittman, R. N. (1998). Apoptotic membrane blebbing is regulated by myosin light chain phosphorylation. *J. Cell Biol.* **140**, 627-636.

Mitchison, T. J. and Cramer, L. P. (1996). Actin-based cell motility and cell locomotion. *Cell* **84**, 371-379.

Pang, K. M., Lee, E. and Knecht, D. A. (1998). Use of a fusion protein between GFP and an actin-binding domain to visualize transient filamentous-actin structures. *Curr. Biol.* **8**, 405-408.

Pasternak, C., Spudich, J. A. and Elson, E. L. (1989). Capping of surface receptors and concomitant cortical tension are generated by conventional myosin. *Nature* **341**, 549-551.

Peckham, M., Miller, G., Wells, C., Zicha, D. and Dunn, G. A. (2001). Specific changes to the mechanism of cell locomotion induced by overexpression of beta-actin. *J. Cell Sci.* **114**, 1367-1377.

Pollard, T. D. and Borisy, G. G. (2003). Cellular motility driven by assembly and disassembly of actin filaments. *Cell* **112**, 453-465.

Ponti, A., Machacek, M., Gupton, S. L., Waterman-Storer, C. M. and Danuser, G. (2004). Two distinct actin networks drive the protrusion of migrating cells. *Science* **305**, 1782-1786.

Raucher, D. and Sheetz, M. P. (2000). Cell spreading and lamellipodial extension rate is regulated by membrane tension. *J. Cell Biol.* **148**, 127-136.

Ridley, A. J., Schwartz, M. A., Burridge, K., Firtel, R. A., Ginsberg, M. H., Borisy, G., Parsons, J. T. and Horwitz, A. R. (2003). Cell migration: integrating signals from front to back. *Science* **302**, 1704-1709.

Sahai, E. and Marshall, C. J. (2003). Differing modes of tumour cell invasion have distinct requirements for Rho/ROCK signalling and extracellular proteolysis. *Nat. Cell Biol.* **5**, 711-719.

Schirenbeck, A., Arasada, R., Bretschneider, T., Schleicher, M. and Faix, J. (2005). Formins and VASPs may co-operate in the formation of filopodia. *Biochem. Soc. Trans.* **33**, 1256-1259.

Schroeder, T. E. (1978). Microvilli on sea urchin eggs: a second burst of elongation. *Dev. Biol.* **64**, 342-346.

Shelden, E. and Knecht, D. A. (1996). Dictyostelium cell shape generation requires myosin II. *Cell Motil. Cytoskeleton* **35**, 59-67.

Shu, S., Liu, X. and Korn, E. D. (2005). Blebbistatin and blebbistatin-inactivated myosin II inhibit myosin II-independent processes in Dictyostelium. *Proc. Natl. Acad. Sci. USA* **102**, 1472-1477.

Straight, A. F., Cheung, A., Limouze, J., Chen, I., Westwood, N. J., Sellers, J. R. and Mitchison, T. J. (2003). Dissecting temporal and spatial control of cytokinesis with a myosin II Inhibitor. *Science* **299**, 1743-1747.

Strasser, G. A., Rahim, N. A., VanderWaal, K. E., Gertler, F. B. and Lanier, L. M. (2004). Arp2/3 is a negative regulator of growth cone translocation. *Neuron* **43**, 81-94.

Strohmeier, R. and Bereiter-Hahn, J. (1987). Hydrostatic pressure in epidermal cells is dependent on Ca-mediated contractions. *J. Cell Sci.* **88**, 631-640.

Sussman, M. (1987). Cultivation and synchronous morphogenesis of Dictyostelium under controlled experimental conditions. *Methods Cell Biol.* **28**, 9-29.

Svitkina, T. M., Verkhovsky, A. B., McQuade, K. M. and Borisy, G. G. (1997). Analysis of the actin-myosin II system in fish epidermal keratocytes: mechanism of cell body translocation. *J. Cell Biol.* **139**, 397-415.

Torgerson, R. R. and McNiven, M. A. (1998). The actin-myosin cytoskeleton mediates reversible agonist-induced membrane blebbing. *J. Cell Sci.* **111**, 2911-2922.

Trinkaus, J. P. (1973). Surface activity and locomotion of Fundulus deep cells during blastula and gastrula stages. *Dev. Biol.* **30**, 69-103.

Uchida, K. S., Kitanishi-Yumura, T. and Yumura, S. (2003). Myosin II contributes to the posterior contraction and the anterior extension during the retraction phase in migrating Dictyostelium cells. *J. Cell Sci.* **116**, 51-60.

Webb, D. J. and Horwitz, A. F. (2003). New dimensions in cell migration. *Nat. Cell Biol.* **5**, 690-692.

Weber, I., Wallraff, E., Albrecht, R. and Gerisch, G. (1995). Motility and substratum adhesion of Dictyostelium wild-type and cytoskeletal mutant cells: a study by RICM/bright-field double-view image analysis. *J. Cell Sci.* **108**, 1519-1530.

Wessels, D., Soll, D. R., Knecht, D., Loomis, W. F., De Lozanne, A. and Spudich, J. (1988). Cell motility and chemotaxis in Dictyostelium amebae lacking myosin heavy chain. *Dev. Biol.* **128**, 164-177.

Yanai, M., Kenyon, C. M., Butler, J. P., Macklem, P. T. and Kelly, S. M. (1996). Intracellular pressure is a motive force for cell motion in Amoeba proteus. *Cell Motil. Cytoskeleton* **33**, 22-29.

Yoshida, K. and Inouye, K. (2001). Myosin II-dependent cylindrical protrusions induced by quinine in Dictyostelium: antagonizing effects of actin polymerization at the leading edge. *J. Cell Sci.* **114**, 2155-2165.